Author Manuscript

Author Manuscript

Author Manuscript

Author Manuscript

HHS Public Access

Author manuscript

Cell Rep. Author manuscript; available in PMC 2025 April 24.

Published in final edited form as:

Cell Rep. 2025 March 25; 44(3): 115422. doi:10.1016/j.celrep.2025.115422.

Transcriptional signatures of hippocampal tau pathology in primary age-related tauopathy and Alzheimer's disease

Genevieve L. Stein-O'Brien[1,2,7,8], **Ryan Palaganas**[1,8], **Ernest M. Meyer**[3], **Javier Redding-Ochoa**[4], **Olga Pletnikova**[4,5], **Haidan Guo**[4], **William R. Bell**[6], **Juan C. Troncoso**[4,7], **Richard L. Huganir**[1,2], **Meaghan Morris**[2,4,9,*]

[1]Department of Neuroscience, Johns Hopkins University School of Medicine, Baltimore, MD 21205, USA

[2]Kavli Neuroscience Discovery Institute, Baltimore, MD 21218, USA

[3]UPMC Hillman Cancer Center Cytometry Facility, University of Pittsburgh, Pittsburgh, PA 15232, USA

[4]Department of Pathology, Johns Hopkins University School of Medicine, Baltimore, MD 21205, USA

[5]Department of Pathology and Anatomical Sciences, University at Buffalo, Buffalo, NY 14203, USA

[6]Department of Pathology and Laboratory Medicine, Indiana University School of Medicine, Indianapolis, IN 46202, USA

[7]Department of Neurology, Johns Hopkins University School of Medicine, Baltimore, MD 21205, USA

[8]These authors contributed equally

[9]Lead contact

SUMMARY

This is an open access article under the CC BY-NC license (http://creativecommons.org/licenses/by-nc/4.0/).

*Correspondence: momalle2@jhmi.edu.

AUTHOR CONTRIBUTIONS

M.M., J.C.T., R.L.H., and G.L.S.-O. designed the study. M.M., J.R.-O., J.C.T., W.R.B., and O.P. participated in tissue selection and pathologic analysis. M.M., H.G., R.P., and E.M.M. developed the protocols and performed data collection. M.M., R.P., and G.L.S.-O. performed the analysis. M.M., R.P., and G.L.S.-O. wrote the manuscript. All authors edited and approved the manuscript.

RESOURCE AVAILABILITY

Lead contact

Further information and requests for resources and reagents should be directed to and will be fulfilled by the lead contact, Meaghan Morris (momalle2@jhmi.edu).

Materials availability

This study did not generate new unique reagents.

Data and code availability

De-identified GeoMx data from human samples generated and analyzed in this study are available in the Neuroscience Multi-omics Data Archive (NeMO), with links for the data and code provided in the key resources table.

DECLARATION OF INTERESTS

The authors declare no competing interests.

SUPPLEMENTAL INFORMATION

Supplemental information can be found online at https://doi.org/10.1016/j.celrep.2025.115422.

Author Manuscript Author Manuscript Author Manuscript Author Manuscript

In primary age-related tauopathy (PART) and Alzheimer's disease (AD), tau aggregates share a similar structure and anatomic distribution, which is distinct from tau pathology in other diseases. However, transcriptional similarities between PART and AD and gene expression changes within tau-pathology-bearing neurons are largely unknown. Using GeoMx spatial transcriptomics, mRNA was quantified in hippocampal neurons with and without tau pathology in PART and AD. Synaptic genes were down-regulated in disease overall but up-regulated in tau-pathology-positive neurons. Two transcriptional signatures were associated with intraneuronal tau, both validated in a cortical AD dataset. Genes in the up-regulated signature were enriched in calcium regulation and synaptic function. Notably, transcriptional changes associated with intraneuronal tau in PART and AD were similar, suggesting a possible mechanistic relationship. These findings highlight the power of molecular analysis stratified by pathology and provide insight into common pathways associated with tau pathology in PART and AD.

Graphical Abstract

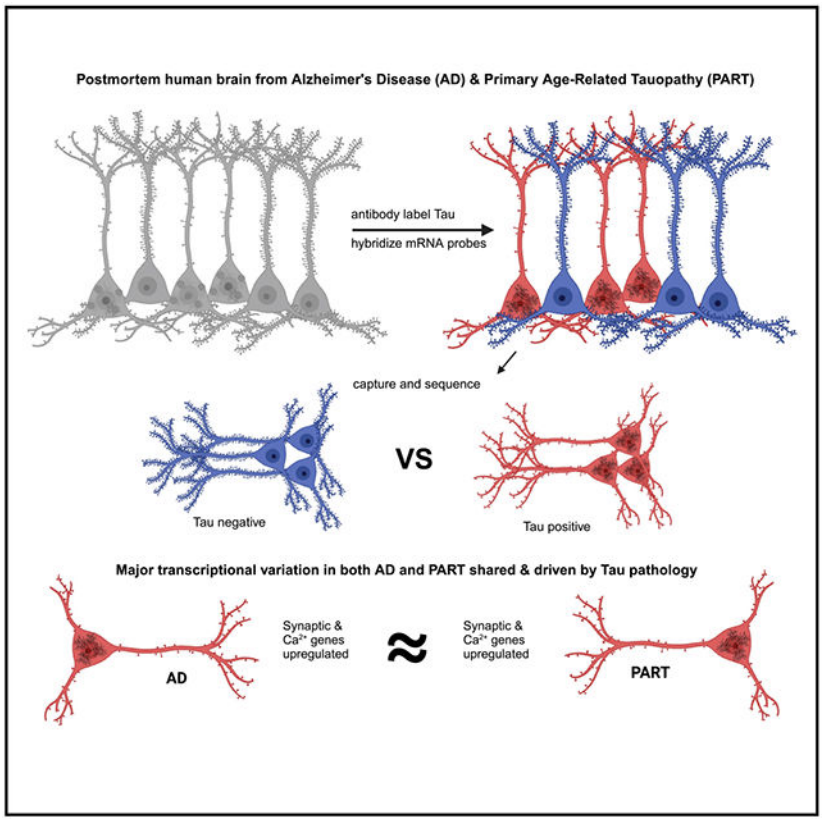

In brief

Stein-O'Brien and Palaganas et al. identify shared transcriptional signatures and synaptic gene changes associated with tau pathology in primary age-related tauopathy and Alzheimer's disease. This study highlights the power of molecular analysis stratified by pathology and provides insight into common pathways associated with tau pathology in aging and Alzheimer's.

Author Manuscript Author Manuscript Author Manuscript Author Manuscript

INTRODUCTION

Tau pathology is present in the brain of nearly all elderly individuals.[1,2] Many show Alzheimer's disease (AD) pathology, defined by tau aggregates in neurons and extracellular amyloid plaques. However, some older individuals show tau aggregates in neurons without plaques, called primary age-related tauopathy (PART).[3,4] The tau pathology in PART and AD is composed of similar hyperphosphorylated tau isoforms and shares a biochemical structure,[5,6] which is not identified in other sporadic tauopathies. The anatomic distribution of tau pathology is so similar in early/mid-stage disease in AD and PART that they share tau pathologic staging.[4,7,8] In both, tau pathology accumulates early in the entorhinal cortex and hippocampus, with later cortical spread. Tau pathology in both is also linked to cognitive impairment.[4,9-13] These similarities led to the hypothesis that PART may represent an early form of AD.[14]

However, the relationship between PART and AD is controversial. By positron emission tomography (PET) imaging, older tau-positive and amyloid-negative individuals, possibly representing PART, do not accumulate amyloid over time and have a different clinical progression from individuals with AD.[15] Despite a similar early distribution of tau pathology, PART cases have a predilection for the hippocampal CA2 region, while AD cases accumulate overall higher levels of tau pathology, which spreads farther across the brain.[4,16-18] Genetic studies have highlighted distinct genetic risk factors for PART and AD.[4,19] Thus, evidence remains inconclusive on whether the two diseases are related.

Little is known about the molecular environment within neurons affected by tau pathology. Tau pathology accumulates only in a subset of neurons.[8,20] Traditional bulk or single-cell RNA methods are not able to segregate neurons with tau pathology from those without. Prior studies looking at pathology-associated transcriptional signals in AD using microdissection and RNA microarrays[21] only identify changes in pre-selected genes. One study developed a cell-sorting-based method for single soma transcriptomics to investigate tau-pathology-associated changes in the cortex in AD,[20] but hippocampal transcriptional changes in PART and AD have not been investigated using unbiased methods. Thus, we leveraged GeoMx spatial transcriptomics to do unbiased gene expression quantification with cell selection using antibody labeling[22,23] in neurons with tau pathology and adjacent neurons without tau pathology in the hippocampus.

Specifically, we quantified transcriptional changes associated with intraneuronal tau pathology in the hippocampal CA1 region in AD and PART. Young controls were included to allow comparison to literature findings in aging and AD.[24] We identified differential gene regulation within neurons with intraneuronal tau pathology in PART and AD, with striking similarities in the tau-associated gene regulation in both conditions.

RESULTS

Transcriptional changes associated with intraneuronal tau pathology

To investigate transcriptional changes associated with intraneuronal tau pathology in AD and PART, we used GeoMx digital spatial profiling (Figure 1A). Hippocampal CA1

Author Manuscript Author Manuscript Author Manuscript Author Manuscript

pyramidal neurons with and without tau pathology were collected from AD, PART, and control cases (Table S1). The CA1 region was chosen due to the high burden of tau pathology and the relatively uniform population of neurons in the CA1 pyramidal layer.[25-28] Neurons were identified by morphology and segmented as tau pathology positive or negative by immunostaining (Figures 1B, 1C, and S1). The numbers of neurons collected were similar across disease segments, defined as neurons within a region of interest with the same tau status (Figure S2A), with good mRNA quantification (Figures S2B and S2C). Quantified mRNA was similar between groups (Figure S2D). mRNA counts did not vary by block age or postmortem interval (Figures S2E and S2F). 2%–10% of the transcriptome was quantified in most segments, resulting in 1,392 quantified genes after quality control and batch correction (Figures S2G and S3). Quantified genes were enriched in excitatory neuronal and synaptic genes but not genes expressed in other cell types (Figures S4A-S4D). When hippocampal cell type markers were examined, markers for excitatory pyramidal neurons were similarly enriched within tau-pathology-positive and -negative neurons without evidence of a cell type bias between groups (Figures S4E and S4F).

The largest variation in gene expression was associated with tau pathology (Figure 1D). Tau-positive neurons were separated from tau-negative neurons by principal-component analysis; however, there was no separation by disease. Multiple differentially expressed genes (DEGs) were identified in tau-positive neurons compared to tau-negative neurons (Figure 1E). In PART, 72 DEGs were identified in tau-positive neurons, with 26 up-regulated and 46 down-regulated (Table S2). In AD, 39 DEGs were identified in tau-positive neurons, with 27 up-regulated and 12 down-regulated (Table S2), a pattern similar to prior findings.[20] Select genes previously shown to be up-regulated in AD cortical tau-positive neurons, including *PRNP* and *APP*, were also up-regulated in hippocampal tau-positive neurons[20] (Figure 1F).

Analysis of DEGs in tau-positive neurons in PART and AD showed several interesting trends. Tau-positive neurons in PART showed differential expression of genes in the amyloid precursor protein (APP) gene family (*APP* and *APLP2*) and APP processing (*PLD3* and *CLSTN1*),[29-31] calcium signaling (*TTYH3, VSNL1, ATP2B1*, and *CALM1*), mitochondrial function (*TXN2, TOMM5, SARDH1, VDAC3*, and *MTCH1*), and mRNA regulation, transcription, and splicing (*PTBP1, PNO1, RPRD1B, PNN*, and *DUX4*). In AD, tau-positive neurons up-regulated pre-synaptic genes (*VAMP2* and *SYT1*) and 14-3-3 family members (*YWHAG, YWHAH*, and *YWHAZ*), which were previously implicated in AD.[32] PART and AD both showed dysregulation of genes involved in apoptosis, endoplasmic reticulum stress, and stress granule pathways (PART: *MTCH1, PEA15, PNMA2, SPIN2B, TXN2*, and *SCAMP5*; AD: *IFITM2, CCDC88B, PTMA, G3BP2*, and *ATF4*).[33]

Synaptic gene regulation associated with intraneuronal tau pathology

Synaptic genes are dysregulated in cortical neurons with tau pathology in AD,[20,24] so we investigated the association of tau pathology with synaptic gene expression in hippocampal neurons in PART and AD. Given the relatively small population of genes quantified, Gene Ontology analysis with background gene correction did not yield enriched pathways.

Author Manuscript Author Manuscript Author Manuscript Author Manuscript

Instead, the intersection of quantified genes and those in the SynGO database[34] was used to examine synaptic gene changes.

First, we confirmed our cohort was representative of aging and AD by showing that our cases replicate the known down-regulation of synaptic genes compared to young controls[24] (Figures 2A-2C; Table S3). Synaptic genes were down-regulated in neurons in PART (Figure 2B, mean log2 fold change: −0.12), with a greater down-regulation in AD (Figure 2C, mean log2 fold change: −0.18), recapitulating prior findings.

When synaptic gene expression was compared in tau-positive vs. tau-negative neurons within disease, the findings were different. Synaptic genes were up-regulated in tau-positive neurons in PART and AD, with a greater magnitude of change in AD (AD, log2 fold change: 0.13; PART, log2 fold change: 0.073; Figures 2D-2F; Table S3). There were no global transcriptional changes in any group (Figures S5A-S5D). Examination of representative synaptic (*SYT1*) and calcium signaling (*CALM3*) genes show the down-regulation of these genes in tau-pathology-negative disease neurons with relative preservation in tau-positive disease neurons (Figures 2G and 2H).

As similar trends were present in tau-positive neurons in PART and AD, we analyzed whether transcriptional changes associated with tau pathology were similar between the two conditions. Plotting the fold change of all quantified genes in tau-positive neurons for PART and AD showed a striking correlation of transcriptional changes between the two conditions (Figure 2I; simple linear regression, $p < 0.0001$, $R^2 = 0.45$), implying that intraneuronal tau pathology is associated with similar transcriptional regulation in PART and AD.

Tau pathology in hippocampal neurons more consistently associated with gene changes compared to amyloid plaques

GeoMx experiments used high-level AD cases to facilitate the identification of amyloid-associated transcriptional changes. Given the lack of an effect of high-level amyloid pathology on tau pathology gene signatures, we investigated this relationship in more detail using an independent cohort of 18 cases with varying neuritic amyloid plaque pathology (Table S4).

Using hybridization chain reaction (HCR),[35] we examined the expression of 4 DEGs in hippocampal CA1 neurons: *SYT1, PRNP, APLP2*, and *CALM1* (Figure 3). Neurons were identified by Neurotrace and classified as tau pathology positive or negative using immunofluorescence (Table S5). Tau pathology was consistently associated with increased DEG expression (tau effect: *SYT1* $p = 0.000131$, *PRNP* $p = 1.88e{-8}$, *CALM1* $p = 3.01e{-5}$, and *APLP2* $p = 0.000665$; mixed-effects linear model), confirming the spatial transcriptomic studies. However, the effect of amyloid was not consistent across DEGs. There was a quadratic relationship of plaque density with baseline expression for *APLP2* (amyloid effect: $p = 0.0222$), but amyloid had no effect on the baseline gene expression of the other genes.

Amyloid plaque density also had an inconsistent effect on the tau-associated changes. There was a cubic relationship between amyloid plaque density and tau pathology for *PRNP* (interaction term: $p = 0.0258$), possibly due to the minimal tau effect in the moderate plaque

Author Manuscript Author Manuscript Author Manuscript Author Manuscript

group. Amyloid neuritic plaques had no interaction with tau pathology in the other genes. So while tau pathology showed a consistent association with DEG changes, there was no consistent effect of amyloid plaques on the tested DEGs.

Transcriptional signatures associated with intraneuronal tau pathology

Coordinated gene association in pattern set (CoGAPS) analysis was performed as an unsupervised analysis to identify patterns of gene expression, followed by PatternMarkers analysis to identify genes associated with each pattern. CoGAPS was used to generate 5 coordinated gene expression patterns (Table S6), two of which were associated with tau pathology. The first pattern showed up-regulation with intraneuronal tau pathology (tau+/AD vs. tau−/AD: $t_{(46)} = 10.52$, $p = 7.94e{-}14$; tau+/PART vs. tau−/PART: $t_{(67)} = 8.4518$, $p = 3.69e{-}12$) (Figures 4A and 4B), with similar changes in PART and AD (tau+/AD vs. tau+/PART: $t_{(56)} = -0.021$, $p = 0.983$; tau−/AD vs. tau−/PART: $t_{(57)} = -0.532$, $p = 0.5967$). This pattern was notable for genes involved in calcium signaling (*CALM1, CALM2, CALM3, CAMKK1*, and *CAMK2B*) and was enriched for SynGO-annotated genes (Figure S6; $p = 0.0001$). Gene Ontology analysis showed enrichment for synaptic signaling (false discovery rate [FDR] = 1.4e–4) and calcium ion transport and cation homeostasis pathways (FDR = 1.4e–4) (Figure 4C; Table S7). The highest enrichment was in the regulation of synaptic vesicle exocytosis (5x enrichment, FDR = 1.5e–4).

The second gene expression pattern was down-regulated in tau-positive neurons (tau+/AD vs. tau−/AD: $t_{(46)} = -10.07$, $p = 3.21e{-}13$; tau+/PART vs. tau−/PART: $t_{(67)} = -13.91$, $p < 2.2e{-}16$) (Figures 4D and 4E), with similar changes in PART and AD (tau+/AD vs. tau+/PART: $t_{(56)} = 0.057$, $p = 0.955$; tau−/AD vs. tau−/PART: $t_{(57)} = -0.011$, $p = 0.991$). The biological significance of this pattern was unclear. Gene Ontology analysis showed no enrichment. Closer examination showed a mix of genes involved in synaptic function, mitochondria, metabolism, and mRNA regulation. While many synaptic genes were in the up-regulated pattern, several were associated with the down-regulated pattern, including glutamate receptors (*GRIA1, GRIA2*, and *GRIN1*) and synaptic signaling genes (*PRKCA, CAMK2A, CACNG8, DLG2/PSD-93*, and *NRXN2*). The other three patterns showed no association with either tau or disease (Figures S5E-S5G).

Shared signatures of intraneuronal tau pathology in cortical neurons

To determine if these transcriptional changes were shared between hippocampal and cortical neurons in AD, we compared our findings to a published single-soma RNA sequencing (RNA-seq) dataset stratified by tau pathology.[20] First, changes in synaptic gene expression were assessed. Genes quantified in the dataset were analyzed for SynGO[34] annotation with neurons grouped as in the original publication.[20] For each excitatory neuron group, the fold change of synaptic genes in tau-positive neurons was compared to the fold change of all quantified genes. Of 9 excitatory neuronal subtypes with tau pathology, 7 groups showed an up-regulation of synaptic genes in tau-positive neurons (Figures 4F and S7). No excitatory neurons showed a down-regulation of synaptic genes in tau-positive neurons.

Second, the use of the CoGAPS hippocampal patterns was assessed in the AD cortical neuron dataset using the transfer learning algorithm ProjectR. The pattern up-regulated in

Author Manuscript Author Manuscript Author Manuscript Author Manuscript

tau-positive hippocampal neurons was also up-regulated in tau-positive cortical neurons in AD ($t_{(91949)} = 70.419$, $p < 2.2e{-}16$) (Figure 4G). Similarly, the down-regulated pattern from tau-positive hippocampal neurons was also down-regulated in tau-positive cortical neurons in AD ($t_{(91949)} = -36.641$, $p < 2.2e{-}16$) (Figure 4H). When excitatory cortical neurons were separated by group (Figures 4I and 4J), the effects of both patterns were most prominent in cortical neurons with high levels of tau pathology (Ex1, Ex2, Ex7, and Ex10).[20]

DISCUSSION

This study used unbiased spatial transcriptomics to measure changes in hippocampal neurons with tau pathology compared to neurons without tau pathology in PART and AD. This is the first study of tau-pathology-associated transcriptional changes in PART. Tau pathology in PART was associated with the dysregulation of genes involved in synaptic function, calcium regulation, apoptosis, and endoplasmic reticulum stress. Intraneuronal tau pathology was also associated with altered expression of APP family genes and genes involved in APP processing,[29-31] critical for amyloid-beta peptide production, which forms plaques in AD. This replicates prior protein and mRNA findings in tau-positive neurons in PART and AD.[20,36,37] The effect of this differential regulation of the genes in the *APP* pathway is uncertain; increased *APP* and decreased *PLD3* favor increased amyloid-beta production. However, increased *CLSTN1* would favor decreased amyloid production via the disruption of *APP* transport.[29] While the net effect of these changes is unclear, these changes suggest a link between tau pathology and altered processing of *APP* in aging.

The transcriptional changes associated with tau pathology in PART and AD are strikingly similar, suggesting a possible relationship between the tau pathologies in both conditions. Currently, the relationship between AD and PART is unclear. Despite similarities in tau aggregates and the progression of the two diseases,[4,5,7,8] there are significant genetic and pathologic differences.[4,17-19,38] The findings in this study show clear transcriptional similarities associated with tau pathology in PART and AD. Given the unique structure of the tau aggregates shared by PART and AD and the shared transcriptional changes, it is possible they share a common pathogenesis of tau pathology.

Non-AD/PART tauopathies are varied diseases with disparate anatomic, cellular, and biochemical features.[39] Most cases of non-AD/PART tauopathies are sporadic and show distinct tau aggregate structures.[5] Tauopathies associated with frontotemporal dementia often aggregate only 3R or 4R isoforms of tau, rather than the mixed 3R/4R aggregates of AD/PART, and show glial tau aggregation.[40] In chronic traumatic encephalopathy, a sporadic tauopathy with mixed 3R/4R aggregates, the tau aggregate structure is distinct from AD/PART.[5,41,42] While this study shows that AD/PART aggregates share a transcriptional signature, future studies will determine whether tauopathies with distinct biochemical structures show distinct transcriptional signatures.

The findings in this study suggest a re-evaluation of our understanding of synaptic regulation in PART and AD. Decreased synaptic gene expression in PART and AD is expected and replicates prior studies.[24,43] However, this decrease was driven by neurons lacking tau pathology. Tau-positive neurons showed increased synaptic gene expression in disease in

Author Manuscript Author Manuscript Author Manuscript Author Manuscript

supervised and unsupervised analyses. These synaptic gene changes were shared by cortical neurons in AD, implying that tau-associated changes are similar across brain regions. A study of more than 400 individuals also showed the increased expression of synaptic pathways in cortical neurons in AD with disease progression,[44] though the technique could not differentiate neurons by pathology.

The significance of this differential synaptic gene regulation in tau-positive and -negative neurons is unclear. Given that neurons with tau pathology in AD lose synaptic spines[45] and tau pathology is associated with evidence of synaptic loss in PART and AD,[16,36,37,46-48] this up-regulation may be compensatory. The down-regulation of synaptic genes in aging, which is exacerbated in AD, is consistent with prior studies.[24] This age-associated down-regulation of synaptic and neuronal genes is similar between humans and macaques,[49] and synaptic gene down-regulation via the *REST* pathway is associated with increased longevity.[50]

While the numbers of up-regulated DEGs were similar in PART and AD, there were more down-regulated genes associated with tau pathology in PART. The tissue quality and gene detection were similar between PART and AD, as was the magnitude of the gene changes, suggesting that this difference may be related to higher variability in AD, or, if replicated, these specific genes may provide insight into processes in which tau pathology diverges between PART and AD.

While there are limitations to this study, the possible implications are important. This study provides support for a hypothesis that tau pathology associated with aging could be mechanistically linked to tau pathology in AD. Many studies have attempted to define how amyloid pathology gives rise to tau aggregates. While studies have identified amyloid as a factor increasing the deposition and spread of tau pathology,[51-55] the link with tau pathology formation remains elusive.[56] This study could support a hypothesis that tau and amyloid pathologies initially form independently, with tau aggregates occurring as an age-related process. Amyloid and tau pathologies then interact in AD to promote the deposition and spread of tau. This relationship between PART and AD tau pathology would also imply that therapeutics targeted at tau-pathology-associated pathways could have efficacy in both conditions. However, larger studies will be needed to more fully evaluate this hypothesis and its implications.

In summary, this study identifies transcriptional signatures and synaptic gene changes associated with intraneuronal tau pathology in PART and AD. Tau-associated transcriptional changes were similar in PART and AD, raising the possibility that the tau aggregates may be mechanistically related. This study also showed that decreased synaptic gene expression in PART and AD is largely driven by neurons lacking tau pathology. These transcriptional changes were replicated in an independent cortical dataset in AD, showing that tau-associated signatures are shared across brain regions. The molecular signatures identified in this study provide insight into shared transcriptional changes in neurons with tau pathology in PART and AD and highlight the importance of accounting for pathology in studies of neurodegeneration.

Author Manuscript Author Manuscript Author Manuscript Author Manuscript

Limitations of the study

This study was designed to evaluate transcriptional signatures associated with tau pathology and not to examine overall differences between AD and PART. While the transcriptional changes were similar in excitatory hippocampal neurons, evaluation of other cell types may show different signatures in the two diseases.[57-60] As is common with new technology, this study is limited by small numbers. While the AD data were validated in an orthogonal dataset and several DEGs confirmed in an independent cohort, larger studies are needed to confirm the findings. Finally, HCR in human postmortem tissue can show low signal with high inter-case variability due to tissue fixation, quality, and postmortem interval[61,62]; however, this was mitigated by using within-case comparison in our analysis.

STAR★METHODS

EXPERIMENTAL MODEL AND STUDY PARTICIPANT DETAILS

All human tissue used in this study was from the Johns Hopkins Brain Resource Center (Baltimore, MD) with a postmortem interval of less than 24 h (Table S1; S4). As tau pathology is a nearly universal feature of aging and most individuals over the age of 50 have tau pathology in the mesial temporal lobe,[1,2] control cases were defined as individuals under the age of 50 years with no evidence of amyloid deposition and no phosphorylated tau in the hippocampus or entorhinal cortex (PHF1, gifted from Dr. Peter Davies). For spatial transcriptomic studies, PART cases were selected to have hippocampal tau pathology (Braak stage II-IV) with no amyloid deposition (Thal 0, CERAD 0). AD cases were selected for AD pathology (Braak V-VI, CERAD frequent) and were age-matched to the PART cases (disease age range, 75–95 years). Spatial transcriptomic studies included 4 control, 6 PART and 6 AD cases. For the hybridization chain reaction (HCR) validation, PART cases were selected to have hippocampal tau pathology (Braak stage IIIV) with no amyloid neuritic plaques (definite/probable PART, Thal 0–1, CERAD 0). AD cases were selected for AD pathology with hippocampal tau pathology and a varying level of neuritic plaque density (Braak II-VI, CERAD sparse, moderate, and frequent). HCR cases included 6 PART cases and 12 AD cases with varying levels of amyloid pathology (3–5 per severity level, Table S4). Cases were balanced for biological sex as much as possible. Of all cases used in this study, 2 were from black individuals (6%), 1 was from an Asian individual (3%), and the remaining 31 individuals were white (91%). All pathologic staging was performed used standard methods.[8,67-69] PART and AD cases were manually reviewed to ensure a sufficient number of tau pathology-positive and tau pathology-negative neurons in the CA1 region for spatial transcriptomic evaluation. Cases were excluded from all categories of this study if there was significant hippocampal degeneration, α-synuclein pathology, TDP-43 pathology, frontotemporal dementia, or acute or chronic ischemic pathology in CA1. All work in this study was approved by the Johns Hopkins Institutional Review Board.

METHOD DETAILS

Antibodies—The AT8 (pS202/T205) phospho-tau (MN1020, Thermo Fisher Scientific, Waltham, MA USA) was used to label tau pathology in this study. Prior to use, the AT8 antibody was concentrated using a centrifugal filter (UFC9010, MilliporeSigma, Burlington,

Author Manuscript Author Manuscript Author Manuscript Author Manuscript

MA USA) then covalently labeled with Alexa 594 using an antibody labeling kit (A20185, Thermo Fisher Scientific, Waltham, MA) according to the manufacturer's instructions.

GeoMx data collection—Formalin-fixed, paraffin-embedded (FFPE) tissue sections were cut at 5 μm thickness from the mid-hippocampus at the level of the lateral geniculate nucleus. Sections were sent to the UPMC Hillman Cancer Center Flow Cytometry Core, where slides were prepared using standard GeoMx protocols with recommended reagents (GMX-PREP-RNAFFPE-12, Nanostring, Seattle, WA USA) and equipment for manual FFPE RNA slide preparation (GeoMx DSP Manual Slide Preparation User Manual, MAN-10150-01) for the Nanostring GeoMx whole transcriptome atlas (HS_R_NGS_WTA_v1.0, GMX-RNA-NGSHuWTA-4, Nanostring, Seattle, WA USA). Antigen retrieval was performed for 20 min at low pressure and 99°C in Tris-EDTA buffer, pH 9.0 (00-4956-58, Thermo Fisher Scientific, Waltham, MA USA). Proteinase K (AM2546, Thermo Fisher Scientific, Waltham, MA USA) was used at a concentration of 0.1ug/mL and tissue was treated for 15 min at 37°C. The labeled AT8 was used at a dilution of 1:800 as a morphology marker for tau pathology. Slides were loaded into the GeoMx DSP instrument and scanned using default instrument settings. Experimenters were blinded to disease group. 2–7 regions of interest (ROIs) (660 × 785 μm) were selected within the CA1 region of the hippocampus per case. Regions were selected to include a minimum of 5 neurons per group (control: no pathologic tau, disease: with and without pathologic tau) while avoiding areas artifactual tissue disruption. The ROI image was exported to Fiji/ImageJ[66], a macro was run to set up the masking of each selected neuronal group (Methods S1), and neurons for each group were manually selected as follows. Pyramidal excitatory neuron cell bodies were identified in the CA1 pyramidal cell layer by their specific morphologic features on SYTO13 labeling (Nanostring, Seattle, WA USA), including large triangular cell body shape, large nucleus, and a prominent nucleolus. Once the cell was identified as a neuron, it was classified as either tau pathology-positive or -negative by whether the cell body contained AT8-positive tau pathology. AT8 signal was not used to identify specific cell types or as a marker of neurons. No lipofuscin quench was used as preliminary experiments with a chemical lipofuscin quenching agent (TrueBlack Plus, Biotium, Fremont, CA USA) showed reduced mRNA counts in treated sections (data not shown). In the absence of a lipofuscin quench, neurons which showed an indeterminate fluorescent signal which were not in the definitely in the positive or negative group by morphology were not included in the collection (Figure S1). The manual selection for each group was exported as a PNG file, and uploaded into the GeoMx ROI as a mask. Selections were collected iteratively by the GeoMx from the ROIs into a 96 well plate (GMX-NGS-SEQ, GMX-DSP-BUFF-KIT, Nanostring, Seattle, WA USA). Collected products were processed and sequenced at the University of Pittsburgh Health Sciences Sequencing Core. Requested sequencing depth was calculated from the total collected area. Collected product was sequenced on an Illumina NextSeq 2000 (Illumina, Inc., San Diego, CA USA). Resulting FASTQ files were decoded and processed into count files using the NanoString GeoMx NGS Pipeline app (version 2.0.21) in the Illumina BaseSpace Sequencing Hub. Count files were uploaded back to the GeoMx DSP instrument indexed with the corresponding slide scans for analysis.

Author Manuscript Author Manuscript Author Manuscript Author Manuscript

Collection and quality control—Collected cells per segment were quantified manually. For each dataset, segment properties were exported from the GeoMx and the deduplicated reads were divided by the cell count for that segment to get the deduplicated reads per cell (Figure S2). mRNA quality and gene expression analysis were performed in R statistical software (version 4.2.2)[63]/RStudio (Posit, Boston, MA USA). Quality analysis was performed using the Nanostring GeoMx packages on Bioconductor (NanoStringNCTools version 1.4.0, GeomxTools version 3.0.1, GeoMxWorkflows version 1.2.0).[64,70,71] All segments passed quality control metrics for percent trimmed reads, stitched reads, aligned reads, and sequencing saturation (>85% all measures). Out of 155 collect segments, 11 were excluded for low gene detection rate (<2% of whole transcriptome atlas), which included 2 AD tau-negative segments and 9 AD tau-positive segments spread across 3 separate AD cases.

Genes were included in the quantitative analysis if the count signal was greater than 2 standard deviations above the GeoMean of the negative control probes in more than 20% of segments. Normalization was done using the calcNormFactors function from the edgeR Bioconductor package as previously described.[72-74] Briefly, the trimmed mean of M-values (TMM) between each pair of samples was calculated to account for differences in library sizes between samples. As day of collection was the greatest source of variation in the data, ComBat batch correction was applied using the 3 separate profiling days as the batch variable.[75,76] Principal components analysis and UMAP dimensionality reduction was performed to visualize the corrected data with regard to slide, sex, and collection (Figure S3).[77] While slide, disease, and tau pathology remained significant sources of variation, sex was not. Additional Combat correction was performed for both collection day and slide on data to be used for downstream dimension reduction analysis, i.e., PCA and CoGAPS analysis.[78] However, because of concerns over confounding and the ability to account for slide effects, the data with only day of collection Combat batch correction was used for differential expression analysis.

HCR probe construction—Custom V3 HCR probes were generated using HCRProbeDesign, a Python-based tool (https://github.com/gofflab/HCRProbeDesign), and a human genome index from Bowtie2 (https://github.com/BenLangmead/bowtie2).[79] All genes had a minimum of 14 split-pair probes distributed across their mRNA sequence (Table S8). Probes oligonucleotides were ordered from Integrated DNA Technologies (Coralville, IA USA) at a stock per-probe concentration of 100 μM.

HCR sample preparation and RNA detection—HCR methods adapted from Schwarzkopf et al., 2021.[35] All solutions were prepared using RNase-free reagents and containers. RNase inhibitor (M0314S, New England Biolabs, Ipswich, MA USA) was added at 1:2000 dilution to critical steps. All incubations were performed in humidified chambers to prevent sample drying. Following hairpin addition, all solutions were maintained below pH 7.4 to preserve signal integrity.

Briefly, 10 μm FFPE sections from the mid-hippocampus at the level of the lateral geniculate nucleus were baked at 60°. Sections were deparaffinized and antigen retrieval was performed using ImmunoDNARetriever with Citrate (BSB 0021, BIO SB, Goleta, CA USA) at 95°C

Author Manuscript Author Manuscript Author Manuscript Author Manuscript

for 15 min. After cooling to 45°C, sections were treated with 1 μg/mL proteinase K (P8107S, New England Biolabs, Ipswich, MA USA) for 15 min at 37°C. Tissue was post-fixed in 4% paraformaldehyde for 5 min and washed in 100 mM Tris pH 7.5 in PBS. For RNA detection, sections were pre-hybridized in 30% probe hybridization buffer (30% formamide, 5x SSC, 9 mM citric acid pH 6.0, 0.1% Tween 20, 50 μg/mL heparin, 1x Denhardt's solution (75-001-8, Thermo Fisher Scientific, Waltham, MA USA), 10% dextran sulfate, 0.5 mg/mL yeast tRNA) at 37°C for 10 min. Probe hybridization was performed overnight at 37°C using 1.6 pmol of each probe set in hybridization buffer. Excess probes were removed through sequential 15-min washes at 37°C with decreasing concentrations of probe wash buffer (100%, 75%, 50%, 25%) in 5x SSCT (5x SSC, 0.1% Tween 20), followed by 100% 5x SSCT. Following probe hybridization, sections were photobleached at 4°C for 72 h using an Amaran LED Monolight (BHPhotoVideo, New York, NY USA) at 30% power. Sections were then pre-amplified in amplification buffer (5x SSC, 0.1% Tween 20, 10% dextran sulfate, 0.5 mg/mL yeast tRNA) for 30 min at room temperature. 6 pmol of hairpin amplifiers (H1 and H2) were used per sample. Hairpins were heated to 95°C for 90 s and allowed to cool to room temperature. Amplification was performed overnight at room temperature. Excess hairpins were removed through multiple washes in 5x SSCT. Following RNA detection, sections were permeabilized with 0.2% Triton X-100 in PBS for 30 min at room temperature. Primary antibody incubation was performed using 1:500 dilution of AT8 phospho-tau antibody (pS202/T205, MN1020, Thermo Fisher Scientific, Waltham, MA USA), followed by washing and secondary antibody incubation using 1:500 antimouse IgG1 Alexa 488 (A21121, Thermo Fisher Scientific, Waltham, MA USA). Sections were counterstained with a 1:50 dilution of NeuroTrace (N21479, Thermo Fisher Scientific, Waltham, MA USA) for 40 min, washed and mounted using a glycerol-based mounting medium (1x PBS in glycerol, 20% n-propyl gallate) and sealed. All HCR slides were imaged on a Leica Mica confocal microscope (Leica, Deerfield, IL) using a 63× objective (HC PL APO CS2 63x/1.40 OIL UV). Imaging acquisition settings were maintained across samples. Researchers were blinded to diagnosis during imaging and image analysis.

QUANTIFICATION AND STATISTICAL ANALYSIS

Differential Gene Expression analysis—Differential gene expression was performed using the lme4 Bioconductor packages in the R programming language as previously described.[66] Briefly, two linear mixed-effect model (LMM) were fit to the data. In both models, slide was included as a random intercept term to account for any technical variation. The first model tested for the presence of tau-negative versus tau-positive neurons in the context of both AD and PART. The second model tested for genes that were differentially expressed between AD, PART, and control. Differentially expressed genes in all analyses were defined as a log2 fold change greater than 0.2 and a false discovery rate-corrected *p* value of less than 0.05. Gene functional annotations were based on GeneCards[33] and ShinyGO (version 0.77)[80] annotations.

Synaptic (SynGO) analysis—The list of quantified genes for hippocampal neurons and the literature cortical single cell dataset were entered into the synaptic gene ontology database (SynGO, https://www.syngoportal.org/)[34] and genes with annotations in SynGO were used to define the class of synaptic genes. The distribution of the fold change for

Author Manuscript Author Manuscript Author Manuscript Author Manuscript

each comparison was plotted in GraphPad Prism 9.4.1 (GraphPad Software, San Diego, CA USA) and fit using a Gaussian model with least-squares regression. The curve fit of synaptic genes were either compared to a theoretical mean of 0 (no change in that comparison) or to the mean of the fit of the distribution of all quantified genes for that dataset using an extra sum of squares F test. Comparison with a theoretical mean of 0 was used in the hippocampal dataset because the total quantified gene changes was not different from 0 for any comparison. Comparison to the overall quantified gene distribution was used for the cortical single cell dataset as this was significantly different from 0 in some cell types.

CoGAPS and PatternMarkers analysis—Coordinated Gene Activity in Pattern Sets (CoGAPS) analysis was applied to the entire log transformed Combat corrected gene expression dataset and run for a range of dimensionalities. Stability of the patterns and the composition of the associated gene expression signatures was assessed as previously described[65] and a dimensionality of five was chosen. Patterns were visualized to assess the ability to distinguish between tau status, sex, collection date, slide, and disease status. *Post hoc* statistics were used to quantify the significance of observed differences in sample weights. The SynGO gene list generated for DEGs was used as input to Fast Gene Set Enrichment Analysis (fsea) for enrichment analysis of the gene loadings for all five patterns.[81] The PatternMarker statistic was calculated on the corresponding gene loadings of all five patterns generating lists for use as data driven biomarkers for each pattern.[78] Gene ontology analysis was conducted using ShinyGO (version 0.77) using the GO Biological Processes database[80] and the list of all quantified genes were used for the background gene set.

Projection analysis—Single soma data[20] from cortical neurons with tau pathology in AD was evaluated for usage of the molecular programs described in all five CoGAPS signatures learned on the GeoMx data (described above) using the projectR Bioconductor package.[65,82] Briefly, the log transformed preprocessed expression data was stratified by excitatory and inhibitory neuron types, subset to those genes common to both datasets, and input to the projectR function along with the feature loadings from all five CoGAPS patterns. The resulting projected pattern weights then quantify the degree to which each molecular program is active in each soma. Difference in activity of these programs were visualized by plotting the projected pattern weights by each cell type, disease state, and Tau status using the annotation reported in Otero-Garcia et al.[20] Post hoc statistics assessing the differential distribution of projected pattern weighs across cell type, disease state, and Tau status were used to quantify the significance of observed differences in the use of each CoGAPS signature and the biological processes associated with it.

Spot detection—To quantify RNA-FISH fluorescent spots, we used an ImageJ[83]-based radial symmetry fluorescent *in-situ* hybridization plug-in (RS-FISH, https://github.com/PreibischLab/RS-FISH).[84] For all genes, a Difference of Gaussians (DoG) sigma of ~1.5 with an anisotropy coefficient of 1.0 was used to threshold spots in the entire image. Random sample consensus (RANSAC) fitting was used to remove outlier spots, with a maximum error of 1.5 pixels, inlier ratio of ~0.4, and support radius of 5 pixels. The spot intensity threshold was manually optimized for each image. Spot intensities were

Author Manuscript Author Manuscript Author Manuscript Author Manuscript

computed using a Gaussian fit on inlier pixels across the entire image intensity range without background subtraction. Double detections were removed if the distance between spots was less than 0.5 pixels. A custom Python script (filter_plot_spots_masks.py) was used to assign detected RNA spots to individual neurons based on the segmentation mask coordinates generated using Cellpose.[85] Valid spots were identified as those falling within the neuron mask boundaries. Each spot was assigned to its corresponding neuron based on the segmentation mask value at the spot coordinates. Total spot count and intensity were collated for each neuron. Normalized spot count was calculated by dividing each spot's intensity by the median spot intensity for that image and gene expression was quantified as spots per 10,000 pixels. Data normality was assessed using Shapiro-Wilk tests and Q-Q plots for each gene across disease severity groups. As gene expression data were not normally distributed, values were log-transformed (log1p) for statistical analysis. Image acquisition and analysis were performed blinded to diagnosis (AD versus PART) and some cases were excluded from the *PRNP/SYT1* analysis due to poor quality RNA signal. Tau pathology positive and negative cells were delineated after segmentation by a board-certified neuropathologist blinded to diagnosis (PART versus AD) and to RNA signal in each cell. Images lacking tau-positive neurons were excluded from the analysis, with a final dataset of 3,189 neurons included (Table S5). Linear mixed-effects models (lmer package[66]) were used to analyze the relationship between gene expression, tau pathology, and amyloid neuritic plaque density. Tau pathology (factor variable) and amyloid plaque density (CERAD score, ordered factor variable) were used as fixed effects with an interaction term and image field as a random effect to account for technical variation between images/cases. Statistical significance was set at $p < 0.05$ for all HCR analyses. For graphical representation of the relative change between tau pathology positive and negative neurons across conditions, relative expression levels were calculated by dividing each neuron's normalized spot count by the mean expression in tau-negative neurons within that image.

Statistical analysis—Gaussian modeling with least-squares regression, simple linear regressions, and extra sum of squares F tests were performed using GraphPad Prism 9.4.1 (GraphPad Software, San Diego, CA USA). Linear mixed model regression, PCA, CoGAPS analysis, projectR analysis, fgsea, t-tests, and anova analysis were performed in the R statistical language version 4.2.2[67]. All statistical details, including statistical tests, experimental numbers and their meaning, definition of center, and dispersion and precision measures can be found in the figure legends, results, and methods.

Supplementary Material

Refer to Web version on PubMed Central for supplementary material.

ACKNOWLEDGMENTS

This work was supported by grant P30 AG066507 with an ADRC Junior Faculty Grant and in part by grants U19 AG033655 and K08 AG07005301 from the National Institutes of Health (NIH)/National Institute on Aging and R00NS122085 from the NIH/National Institute of Neurological Disorders and Stroke. This project used the UPMC Hillman Cancer Center Cytometry Facility, which is supported in part by award P30 CA047904 (National Cancer Institute/NIH). This research was supported in part by the Intramural Research Program, National Institute on Aging, NIH. We would also like to acknowledge Prajan Divakar, Nanostring, for technical support. The macro code (Methods S1) was provided courtesy of Research and Development at Nanostring (Seattle, WA).

Author Manuscript Author Manuscript Author Manuscript Author Manuscript

REFERENCES

1. Pletnikova O, Kageyama Y, Rudow G, LaClair KD, Albert M, Crain BJ, Tian J, Fowler D, and Troncoso JC (2018). The spectrum of preclinical Alzheimer's disease pathology and its modulation by ApoE genotype. Neurobiol. Aging 71, 72–80. 10.1016/j.neurobiolaging.2018.07.007. [PubMed: 30099348]
2. Braak H, Thal DR, Ghebremedhin E, and Del Tredici K (2011). Stages of the pathologic process in Alzheimer disease: age categories from 1 to 100 years. J. Neuropathol. Exp. Neurol 70, 960–969. 10.1097/NEN.0b013e318232a379. [PubMed: 22002422]
3. Kim D, Kim HS, Choi SM, Kim BC, Lee MC, Lee KH, and Lee JH (2019). Primary Age-Related Tauopathy: An Elderly Brain Pathology Frequently Encountered during Autopsy. J. Pathol. Transl. Med 53, 159–163. 10.4132/jptm.2019.03.14. [PubMed: 30887795]
4. Crary JF, Trojanowski JQ, Schneider JA, Abisambra JF, Abner EL, Alafuzoff I, Arnold SE, Attems J, Beach TG, Bigio EH, et al. (2014). Primary age-related tauopathy (PART): a common pathology associated with human aging. Acta Neuropathol. 128, 755–766. 10.1007/s00401-014-1349-0. [PubMed: 25348064]
5. Shi Y, Zhang W, Yang Y, Murzin AG, Falcon B, Kotecha A, van Beers M, Tarutani A, Kametani F, Garringer HJ, et al. (2021). Structure-based classification of tauopathies. Nature 598, 359–363. 10.1038/s41586-021-03911-7. [PubMed: 34588692]
6. Shi Y, Murzin AG, Falcon B, Epstein A, Machin J, Tempest P, Newell KL, Vidal R, Garringer HJ, Sahara N, et al. (2021). Cryo-EM structures of tau filaments from Alzheimer's disease with PET ligand APN-1607. Acta Neuropathol. 141, 697–708. 10.1007/s00401-021-02294-3. [PubMed: 33723967]
7. Braak H, and Braak E (1991). Neuropathological stageing of Alzheimer-related changes. Acta Neuropathol. 82, 239–259. 10.1007/BF00308809. [PubMed: 1759558]
8. Braak H, Alafuzoff I, Arzberger T, Kretzschmar H, and Del Tredici K (2006). Staging of Alzheimer disease-associated neurofibrillary pathology using paraffin sections and immunocytochemistry. Acta Neuropathol. 112, 389–404. 10.1007/s00401-006-0127-z. [PubMed: 16906426]
9. Bancher C, Braak H, Fischer P, and Jellinger KA (1993). Neuropathological staging of Alzheimer lesions and intellectual status in Alzheimer's and Parkinson's disease patients. Neurosci. Lett 162, 179–182. 10.1016/0304-3940(93)90590-h. [PubMed: 8121624]
10. Jefferson-George KS, Wolk DA, Lee EB, and McMillan CT (2017). Cognitive decline associated with pathological burden in primary age-related tauopathy. Alzheimers Dement. 13, 1048–1053. 10.1016/j.jalz.2017.01.028. [PubMed: 28322204]
11. Besser LM, Crary JF, Mock C, and Kukull WA (2017). Comparison of symptomatic and asymptomatic persons with primary age-related tauopathy. Neurology 89, 1707–1715. 10.1212/WNL.0000000000004521. [PubMed: 28916532]
12. Bell WR, An Y, Kageyama Y, English C, Rudow GL, Pletnikova O, Thambisetty M, O'Brien R, Moghekar AR, Albert MS, et al. (2019). Neuropathologic, genetic, and longitudinal cognitive profiles in primary age-related tauopathy (PART) and Alzheimer's disease. Alzheimers Dement. 15, 8–16. 10.1016/j.jalz.2018.07.215. [PubMed: 30465754]
13. Iida MA, Farrell K, Walker JM, Richardson TE, Marx GA, Bryce CH, Purohit D, Ayalon G, Beach TG, Bigio EH, et al. (2021). Predictors of cognitive impairment in primary age-related tauopathy: an autopsy study. Acta Neuropathol. Commun 9, 134. 10.1186/s40478-021-01233-3. [PubMed: 34353357]
14. van der Kant R, Goldstein LSB, and Ossenkoppele R (2020). Amyloid-beta-independent regulators of tau pathology in Alzheimer disease. Nat. Rev. Neurosci 21, 21–35. 10.1038/s41583-019-0240-3. [PubMed: 31780819]
15. Costoya-Sanchez A, Moscoso A, Silva-Rodriguez J, Pontecorvo MJ, Devous MDS, Aguiar P, Scholl M, Grothe MJ, Alzheimer's Disease Neuroimaging, I., and the Harvard Aging Brain, S. (2023). Increased Medial Temporal Tau Positron Emission Tomography Uptake in the Absence of Amyloid-beta Positivity. JAMA Neurol. 80, 1051–1061. 10.1001/jamaneurol.2023.2560. [PubMed: 37578787]

Author Manuscript Author Manuscript Author Manuscript Author Manuscript

16. Morris M, Coste GI, Redding-Ochoa J, Guo H, Graves AR, Troncoso JC, and Huganir RL (2023). Hippocampal synaptic alterations associated with tau pathology in primary age-related tauopathy. J. Neuropathol. Exp. Neurol 82, 836–844. 10.1093/jnen/nlad064. [PubMed: 37595576]

17. Walker JM, Fudym Y, Farrell K, Iida MA, Bieniek KF, Seshadri S, White CL, Crary JF, and Richardson TE (2021). Asymmetry of Hippocampal Tau Pathology in Primary Age-Related Tauopathy and Alzheimer Disease. J. Neuropathol. Exp. Neurol 80, 436–445. 10.1093/jnen/nlab032. [PubMed: 33860327]

18. Walker JM, Richardson TE, Farrell K, Iida MA, Foong C, Shang P, Attems J, Ayalon G, Beach TG, Bigio EH, et al. (2021). Early Selective Vulnerability of the CA2 Hippocampal Subfield in Primary Age-Related Tauopathy. J. Neuropathol. Exp. Neurol 80, 102–111. 10.1093/jnen/nlaa153. [PubMed: 33367843]

19. Farrell K, Kim S, Han N, Iida MA, Gonzalez EM, Otero-Garcia M, Walker JM, Richardson TE, Renton AE, Andrews SJ, et al. (2022). Genome-wide association study and functional validation implicates JADE1 in tauopathy. Acta Neuropathol. 143, 33–53. 10.1007/s00401-021-02379-z. [PubMed: 34719765]

20. Otero-Garcia M, Mahajani SU, Wakhloo D, Tang W, Xue YQ, Morabito S, Pan J, Oberhauser J, Madira AE, Shakouri T, et al. (2022). Molecular signatures underlying neurofibrillary tangle susceptibility in Alzheimer's disease. Neuron 110, 2929–2948. 10.1016/j.neuron.2022.06.021. [PubMed: 35882228]

21. Dunckley T, Beach TG, Ramsey KE, Grover A, Mastroeni D, Walker DG, LaFleur BJ, Coon KD, Brown KM, Caselli R, et al. (2006). Gene expression correlates of neurofibrillary tangles in Alzheimer's disease. Neurobiol. Aging 27, 1359–1371. 10.1016/j.neurobiolaging.2005.08.013. [PubMed: 16242812]

22. Zollinger DR, Lingle SE, Sorg K, Beechem JM, and Merritt CR (2020). GeoMx RNA Assay: High Multiplex, Digital, Spatial Analysis of RNA in FFPE Tissue. Methods Mol. Biol 2148, 331–345. 10.1007/978-1-0716-0623-0_21. [PubMed: 32394392]

23. Roberts K, Aivazidis A, Kleshchevnikov V, Li T, Fropf R, Rhodes M, Beechem JM, Hemberg M, and Bayraktar OA (2021). Transcriptome-wide spatial RNA profiling maps the cellular architecture of the developing human neocortexPreprint. bioRxiv 2021, 2003.2020.436265. 10.1101/2021.03.20.436265.

24. Berchtold NC, Coleman PD, Cribbs DH, Rogers J, Gillen DL, and Cotman CW (2013). Synaptic genes are extensively downregulated across multiple brain regions in normal human aging and Alzheimer's disease. Neurobiol. Aging 34, 1653–1661. 10.1016/j.neurobiolaging.2012.11.024. [PubMed: 23273601]

25. Cembrowski MS, Bachman JL, Wang L, Sugino K, Shields BC, and Spruston N (2016). Spatial Gene-Expression Gradients Underlie Prominent Heterogeneity of CA1 Pyramidal Neurons. Neuron 89, 351–368. 10.1016/j.neuron.2015.12.013. [PubMed: 26777276]

26. Siletti K, Hodge R, Mossi Albiach A, Lee KW, Ding SL, Hu L, Lönnerberg P, Bakken T, Casper T, Clark M, et al. (2023). Transcriptomic diversity of cell types across the adult human brain. Science 382, eadd7046. 10.1126/science.add7046. [PubMed: 37824663]

27. Ayhan F, Kulkarni A, Berto S, Sivaprakasam K, Douglas C, Lega BC, and Konopka G (2021). Resolving cellular and molecular diversity along the hippocampal anterior-to-posterior axis in humans. Neuron 109, 2091–2105. 10.1016/j.neuron.2021.05.003. [PubMed: 34051145]

28. Habib N, Avraham-Davidi I, Basu A, Burks T, Shekhar K, Hofree M, Choudhury SR, Aguet F, Gelfand E, Ardlie K, et al. (2017). Massively parallel single-nucleus RNA-seq with DroNc-seq. Nat. Methods 14, 955–958. 10.1038/nmeth.4407. [PubMed: 28846088]

29. Vagnoni A, Perkinton MS, Gray EH, Francis PT, Noble W, and Miller CCJ (2012). Calsyntenin-1 mediates axonal transport of the amyloid precursor protein and regulates Abeta production. Hum. Mol. Genet 21, 2845–2854. 10.1093/hmg/dds109. [PubMed: 22434822]

30. Bayer TA, Cappai R, Masters CL, Beyreuther K, and Multhaup G (1999). It all sticks together–the APP-related family of proteins and Alzheimer's disease. Mol. Psychiatr 4, 524–528. 10.1038/sj.mp.4000552.

31. Cruchaga C, Karch CM, Jin SC, Benitez BA, Cai Y, Guerreiro R, Harari O, Norton J, Budde J, Bertelsen S, et al. (2014). Rare coding variants in the phospholipase D3 gene confer risk for Alzheimer's disease. Nature 505, 550–554. 10.1038/nature12825. [PubMed: 24336208]

Author Manuscript Author Manuscript Author Manuscript Author Manuscript

32. Foote M, and Zhou Y (2012). 14-3-3 proteins in neurological disorders. Int. J. Biochem. Mol. Biol 3, 152–164. [PubMed: 22773956]
33. Stelzer G, Rosen N, Plaschkes I, Zimmerman S, Twik M, Fishilevich S, Stein TI, Nudel R, Lieder I, Mazor Y, et al. (2016). The GeneCards Suite: From Gene Data Mining to Disease Genome Sequence Analyses. Curr. Protoc. Bioinformatics 54, 1.30.1–1.30.33. 10.1002/cpbi.5.
34. Koopmans F, van Nierop P, Andres-Alonso M, Byrnes A, Cijsouw T, Coba MP, Cornelisse LN, Farrell RJ, Goldschmidt HL, Howrigan DP, et al. (2019). SynGO: An Evidence-Based, Expert-Curated Knowledge Base for the Synapse. Neuron 103, 217–234. 10.1016/j.neuron.2019.05.002. [PubMed: 31171447]
35. Schwarzkopf M, Liu MC, Schulte SJ, Ives R, Husain N, Choi HMT, and Pierce NA (2021). Hybridization chain reaction enables a unified approach to multiplexed, quantitative, high-resolution immunohistochemistry and in situ hybridization. Development 148, dev199847. 10.1242/dev.199847. [PubMed: 35020875]
36. Walker JM, Orr ME, Orr TC, Thorn EL, Christie TD, Yokoda RT, Vij M, Ehrenberg AJ, Marx GA, McKenzie AT, et al. (2024). Spatial proteomics of hippocampal subfield-specific pathology in Alzheimer's disease and primary age-related tauopathy. Alzheimers Dement. 20, 783–797. 10.1002/alz.13484. [PubMed: 37777848]
37. Walker JM, Kazempour Dehkordi S, Fracassi A, Vanschoiack A, Pavenko A, Taglialatela G, Woltjer R, Richardson TE, Zare H, and Orr ME (2022). Differential protein expression in the hippocampi of resilient individuals identified by digital spatial profiling. Acta Neuropathol. Commun 10, 23. 10.1186/s40478-022-01324-9. [PubMed: 35164877]
38. Morris M, Coste GI, Redding-Ochoa J, Guo H, Graves AR, Troncoso JC, and Huganir RL (2023). Hippocampal Synaptic Alterations Associated with Tau Pathology in Primary Age-Related Tauopathy. medRxiv 2023.2002.2022, 2023.02.22.23286323. 10.1101/2023.02.22.23286323.
39. Chung DEC, Roemer S, Petrucelli L, and Dickson DW (2021). Cellular and pathological heterogeneity of primary tauopathies. Mol. Neurodegener 16, 57. 10.1186/s13024-021-00476-x. [PubMed: 34425874]
40. Bigio EH (2013). Making the diagnosis of frontotemporal lobar degeneration. Arch. Pathol. Lab Med 137, 314–325. 10.5858/arpa.2012-0075-RA. [PubMed: 23451743]
41. Bieniek KF, Cairns NJ, Crary JF, Dickson DW, Folkerth RD, Keene CD, Litvan I, Perl DP, Stein TD, Vonsattel JP, et al. (2021). The Second NINDS/NIBIB Consensus Meeting to Define Neuropathological Criteria for the Diagnosis of Chronic Traumatic Encephalopathy. J. Neuropathol. Exp. Neurol 80, 210–219. 10.1093/jnen/nlab001. [PubMed: 33611507]
42. Falcon B, Zivanov J, Zhang W, Murzin AG, Garringer HJ, Vidal R, Crowther RA, Newell KL, Ghetti B, Goedert M, and Scheres SHW (2019). Novel tau filament fold in chronic traumatic encephalopathy encloses hydrophobic molecules. Nature 568, 420–423. 10.1038/s41586-019-1026-5. [PubMed: 30894745]
43. Counts SE, Alldred MJ, Che S, Ginsberg SD, and Mufson EJ (2014). Synaptic gene dysregulation within hippocampal CA1 pyramidal neurons in mild cognitive impairment. Neuropharmacology 79, 172–179. 10.1016/j.neuropharm.2013.10.018. [PubMed: 24445080]
44. Mathys H, Peng Z, Boix CA, Victor MB, Leary N, Babu S, Abdelhady G, Jiang X, Ng AP, Ghafari K, et al. (2023). Single-cell atlas reveals correlates of high cognitive function, dementia, and resilience to Alzheimer's disease pathology. Cell 186, 4365–4385. 10.1016/j.cell.2023.08.039. [PubMed: 37774677]
45. Merino-Serrais P, Benavides-Piccione R, Blazquez-Llorca L, Kastanauskaite A, Rábano A, Avila J, and DeFelipe J (2013). The influence of phospho-tau on dendritic spines of cortical pyramidal neurons in patients with Alzheimer's disease. Brain 136, 1913–1928. 10.1093/brain/awt088. [PubMed: 23715095]
46. Wakabayashi K, Honer WG, and Masliah E (1994). Synapse alterations in the hippocampal-entorhinal formation in Alzheimer's disease with and without Lewy body disease. Brain Res. 667, 24–32. 10.1016/0006-8993(94)91709-4. [PubMed: 7895080]
47. Coomans EM, Schoonhoven DN, Tuncel H, Verfaillie SCJ, Wolters EE, Boellaard R, Ossenkoppele R, den Braber A, Scheper W, Schober P, et al. (2021). In vivo tau pathology is associated with synaptic loss and altered synaptic function. Alzheimers Res. Ther 13, 35. 10.1186/s13195-021-00772-0. [PubMed: 33546722]

Author Manuscript Author Manuscript Author Manuscript Author Manuscript

48. Mecca AP, Chen MK, O'Dell RS, Naganawa M, Toyonaga T, Godek TA, Harris JE, Bartlett HH, Zhao W, Banks ER, et al. (2022). Association of entorhinal cortical tau deposition and hippocampal synaptic density in older individuals with normal cognition and early Alzheimer's disease. Neurobiol. Aging 111, 44–53. 10.1016/j.neurobiolaging.2021.11.004. [PubMed: 34963063]

49. Loerch PM, Lu T, Dakin KA, Vann JM, Isaacs A, Geula C, Wang J, Pan Y, Gabuzda DH, Li C, et al. (2008). Evolution of the aging brain transcriptome and synaptic regulation. PLoS One 3, e3329. 10.1371/journal.pone.0003329. [PubMed: 18830410]

50. Zullo JM, Drake D, Aron L, O'Hern P, Dhamne SC, Davidsohn N, Mao CA, Klein WH, Rotenberg A, Bennett DA, et al. (2019). Regulation of lifespan by neural excitation and REST. Nature 574, 359–364. 10.1038/s41586-019-1647-8. [PubMed: 31619788]

51. Li T, Braunstein KE, Zhang J, Lau A, Sibener L, Deeble C, and Wong PC (2016). The neuritic plaque facilitates pathological conversion of tau in an Alzheimer's disease mouse model. Nat. Commun 7, 12082. 10.1038/ncomms12082. [PubMed: 27373369]

52. Price JL, and Morris JC (1999). Tangles and plaques in nondemented aging and "preclinical" Alzheimer's disease. Ann. Neurol 45, 358–368. 10.1002/1531-8249(199903)45:3<358::aid-ana12>3.0.co;2-x. [PubMed: 10072051]

53. Dore V, Krishnadas N, Bourgeat P, Huang K, Li S, Burnham S, Masters CL, Fripp J, Villemagne VL, and Rowe CC (2021). Relationship between amyloid and tau levels and its impact on tau spreading. Eur. J. Nucl. Med. Mol. Imag 48, 2225–2232. 10.1007/s00259-021-05191-9.

54. Lee WJ, Brown JA, Kim HR, La Joie R, Cho H, Lyoo CH, Rabinovici GD, Seong JK, Seeley WW, and Alzheimer's Disease Neuroimaging I (2022). Regional Abeta-tau interactions promote onset and acceleration of Alzheimer's disease tau spreading. Neuron 110, 1932–1943. 10.1016/j.neuron.2022.03.034. [PubMed: 35443153]

55. Adams JN, Maass A, Harrison TM, Baker SL, and Jagust WJ (2019). Cortical tau deposition follows patterns of entorhinal functional connectivity in aging. Elife 8, e49132. 10.7554/eLife.49132. [PubMed: 31475904]

56. Busche MA, and Hyman BT (2020). Synergy between amyloid-beta and tau in Alzheimer's disease. Nat. Neurosci 23, 1183–1193. 10.1038/s41593-020-0687-6. [PubMed: 32778792]

57. Hashemiaghdam A, and Mroczek M (2020). Microglia heterogeneity and neurodegeneration: The emerging paradigm of the role of immunity in Alzheimer's disease. J. Neuroimmunol 341, 577185. 10.1016/j.jneuroim.2020.577185. [PubMed: 32045774]

58. Su Y, Zhou Y, Bennett ML, Li S, Carceles-Cordon M, Lu L, Huh S, Jimenez-Cyrus D, Kennedy BC, Kessler SK, et al. (2022). A single-cell transcriptome atlas of glial diversity in the human hippocampus across the postnatal lifespan. Cell Stem Cell 29, 1594–1610. 10.1016/j.stem.2022.09.010. [PubMed: 36332572]

59. Prokop S, Miller KR, Labra SR, Pitkin RM, Hoxha K, Narasimhan S, Changolkar L, Rosenbloom A, Lee VMY, and Trojanowski JQ (2019). Impact of TREM2 risk variants on brain region-specific immune activation and plaque microenvironment in Alzheimer's disease patient brain samples. Acta Neuropathol. 138, 613–630. 10.1007/s00401-019-02048-2. [PubMed: 31350575]

60. Lau SF, Cao H, Fu AKY, and Ip NY (2020). Single-nucleus transcriptome analysis reveals dysregulation of angiogenic endothelial cells and neuroprotective glia in Alzheimer's disease. Proc. Natl. Acad. Sci. USA 117, 25800–25809. 10.1073/pnas.2008762117. [PubMed: 32989152]

61. Hurler CA, Liebscher S, Arzberger T, and Jäkel S (2024). Impact of fixation duration on messenger RNA detectability in human formalin-fixed paraffin-embedded brain tissue. Brain Commun. 6, fcae430. 10.1093/braincomms/fcae430. [PubMed: 39659968]

62. Tian J, Lam TG, Ross SK, Ciener B, Leskinen S, Sivakumar S, Bennett DA, Menon V, McKhann GM, Runnels A, and Teich AF (2025). An analysis of RNA quality metrics in human brain tissue. J. Neuropathol. Exp. Neurol 84, 236–243. 10.1093/jnen/nlae132. [PubMed: 39715490]

63. R Core Team (2023). R: A Language and Environment for Statistical Computing (R Foundation for Statistical Computing).

64. Ortogero N, Yang Z, Vitancol R, Griswold M, and Henderson D (2022). GeomxTools: NanoString GeoMx Tools. https://github.com/Nanostring-Biostats/GeomxTools.

Author Manuscript Author Manuscript Author Manuscript Author Manuscript

65. Stein-O'Brien GL, Clark BS, Sherman T, Zibetti C, Hu Q, Sealfon R, Liu S, Qian J, Colantuoni C, Blackshaw S, et al. (2019). Decomposing Cell Identity for Transfer Learning across Cellular Measurements, Platforms, Tissues, and Species. Cell Syst 8, 395–411. 10.1016/j.cels.2019.04.004. [PubMed: 31121116]
66. Kuznetsova A, Brockhoff PB, and Christensen RHB (2017). lmerTest Package: Tests in Linear Mixed Effects Models. J. Stat. Software 82, 1–26. 10.18637/jss.v082.i13.
67. Thal DR, Rüb U, Orantes M, and Braak H (2002). Phases of A beta-deposition in the human brain and its relevance for the development of AD. Neurology 58, 1791–1800. 10.1212/wnl.58.12.1791. [PubMed: 12084879]
68. Mirra SS, Heyman A, McKeel D, Sumi SM, Crain BJ, Brownlee LM, Vogel FS, Hughes JP, van Belle G, and Berg L (1991). The Consortium to Establish a Registry for Alzheimer's Disease (CERAD). Part II. Standardization of the neuropathologic assessment of Alzheimer's disease. Neurology 41, 479–486. 10.1212/wnl.41.4.479. [PubMed: 2011243]
69. Hyman BT, Phelps CH, Beach TG, Bigio EH, Cairns NJ, Carrillo MC, Dickson DW, Duyckaerts C, Frosch MP, Masliah E, et al. (2012). National Institute on Aging-Alzheimer's Association guidelines for the neuropathologic assessment of Alzheimer's disease. Alzheimers Dement. 8, 1–13. 10.1016/j.jalz.2011.10.007. [PubMed: 22265587]
70. Reeves J, Divakar P, Ortogero N, Griswold M, Yang Z, Zimmerman S, Vitancol R, and Henderson D (2022). GeoMxWorkflows: GeoMx Digital Spatial Profiler (DSP) data analysis workflows. 10.18129/B9.bioc.GeoMxWorkflows
71. Aboyoun P. (2022). NanoStringNCTools: NanoString nCounter Tools. 10.18129/B9.bioc.NanoStringNCTools
72. Robinson MD, McCarthy DJ, and Smyth GK (2010). edgeR: a Bioconductor package for differential expression analysis of digital gene expression data. Bioinformatics 26, 139–140. 10.1093/bioinformatics/btp616. [PubMed: 19910308]
73. McCarthy DJ, Chen Y, and Smyth GK (2012). Differential expression analysis of multifactor RNA-Seq experiments with respect to biological variation. Nucleic Acids Res. 40, 4288–4297. 10.1093/nar/gks042. [PubMed: 22287627]
74. Chen Y, Lun ATL, and Smyth GK (2016). From reads to genes to pathways: differential expression analysis of RNA-Seq experiments using Rsubread and the edgeR quasi-likelihood pipeline. F1000Res. 5, 1438. 10.12688/f1000research.8987.2. [PubMed: 27508061]
75. Johnson WE, Li C, and Rabinovic A (2007). Adjusting batch effects in microarray expression data using empirical Bayes methods. Biostatistics 8, 118–127. 10.1093/biostatistics/kxj037. [PubMed: 16632515]
76. Zhang Y, Parmigiani G, and Johnson WE (2020). ComBat-seq: batch effect adjustment for RNA-seq count data. NAR Genom. Bioinform 2, lqaa078. 10.1093/nargab/lqaa078. [PubMed: 33015620]
77. McInnes L, Healy J, and Melville J (2020). UMAP: Uniform Manifold Approximation and Projection for Dimension Reduction. https://github.com/lmcinnes/umap.
78. Stein-O'Brien GL, Carey JL, Lee WS, Considine M, Favorov AV, Flam E, Guo T, Li S, Marchionni L, Sherman T, et al. (2017). PatternMarkers & GWCoGAPS for novel data-driven biomarkers via whole transcriptome NMF. Bioinformatics 33, 1892–1894. 10.1093/bioinformatics/btx058. [PubMed: 28174896]
79. Langmead B, and Salzberg SL (2012). Fast gapped-read alignment with Bowtie 2. Nat. Methods 9, 357–359. 10.1038/nmeth.1923. [PubMed: 22388286]
80. Ge SX, Jung D, and Yao R (2020). ShinyGO: a graphical gene-set enrichment tool for animals and plants. Bioinformatics 36, 2628–2629. 10.1093/bioinformatics/btz931. [PubMed: 31882993]
81. Korotkevich G, Sukhov V, Budin N, Shpak B, Artyomov MN, and Sergushichev A (2021). Fast gene set enrichment analysisPreprint. bioRxiv, 060012. 10.1101/060012.
82. Sharma G, Colantuoni C, Goff LA, Fertig EJ, and Stein-O'Brien G (2020). projectR: an R/Bioconductor package for transfer learning via PCA, NMF, correlation and clustering. Bioinformatics 36, 3592–3593. 10.1093/bioinformatics/btaa183. [PubMed: 32167521]

Author Manuscript Author Manuscript Author Manuscript Author Manuscript

83. Schindelin J, Arganda-Carreras I, Frise E, Kaynig V, Longair M, Pietzsch T, Preibisch S, Rueden C, Saalfeld S, Schmid B, et al. (2012). Fiji: an open-source platform for biological-image analysis. Nat. Methods 9, 676–682. 10.1038/nmeth.2019. [PubMed: 22743772]

84. Bahry E, Breimann L, Zouinkhi M, Epstein L, Kolyvanov K, Mamrak N, King B, Long X, Harrington KIS, Lionnet T, and Preibisch S (2022). RS-FISH: precise, interactive, fast, and scalable FISH spot detection. Nat. Methods 19, 1563–1567. 10.1038/s41592-022-01669-y. [PubMed: 36396787]

85. Pachitariu M, and Stringer C (2022). Cellpose 2.0: how to train your own model. Nat. Methods 19, 1634–1641. 10.1038/s41592-022-01663-4. [PubMed: 36344832]

Author Manuscript Author Manuscript Author Manuscript Author Manuscript

Highlights

- Transcriptional changes in CA1 neurons are driven by tau pathology in aging and Alzheimer's
- Synaptic and calcium regulatory gene expression is increased in neurons with tau pathology
- Tau pathology RNA signatures are shared in Alzheimer's and primary age-related tauopathy

Author Manuscript Author Manuscript Author Manuscript Author Manuscript

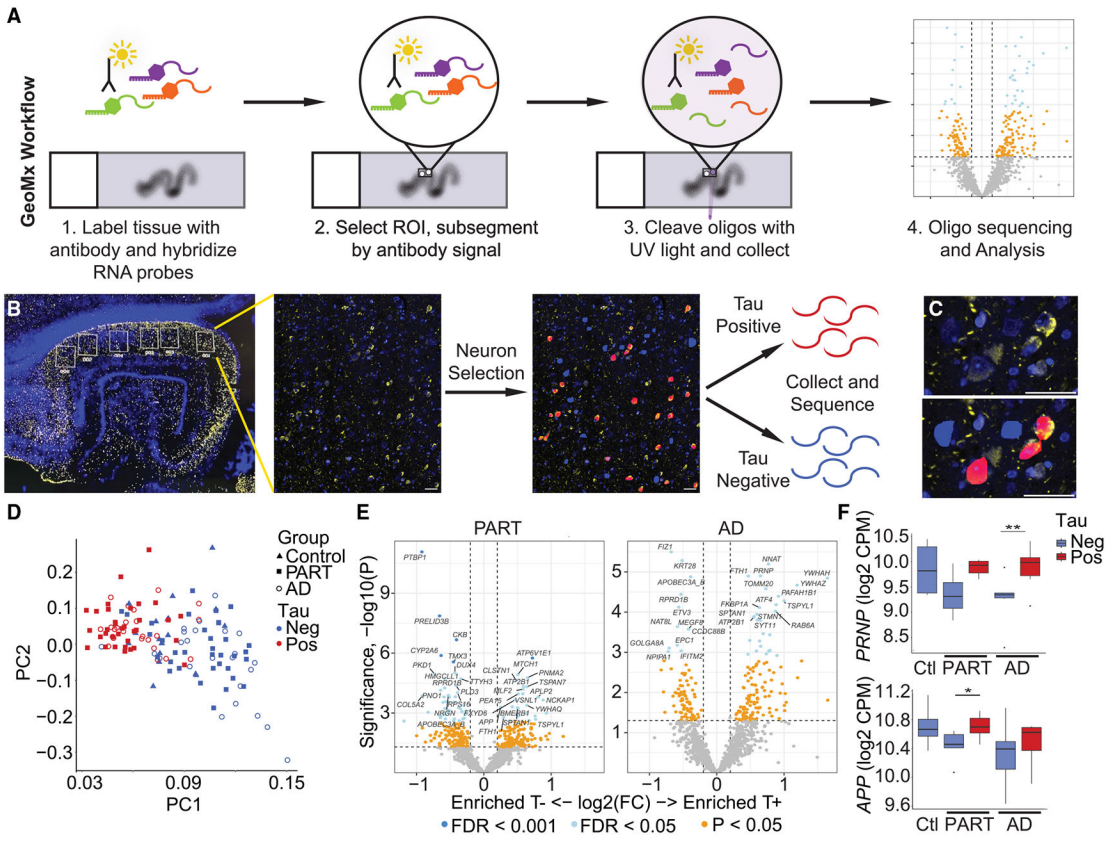

Figure 1. Transcriptional changes associated with tau pathology in PART and AD

(A) GeoMx workflow: tissue is labeled with antibodies and mRNA probes. A region of interest (ROI) is selected and then segmented by antibody labeling. A 10 μm ultraviolet light cleaves the probe barcodes, which are iteratively collected, sequenced, and analyzed from each segment.

(B) Hippocampal sections stained for tau pathology (yellow, AT8) and nucleic acid (blue, SYTO13). ROIs were selected within CA1, segmented, and masked for neurons with (red, tau positive) or without (blue, tau negative) tau pathology. Transcript-specific barcodes were sequenced from each segment.

(C) Higher power of positive (red) and negative (blue) neurons.

(D) Principal-component analysis with PC1 accounting for 99.741% and PC2 accounting for 0.217% of the variance.

(E) Differentially expressed genes in tau-positive neurons.

(F) Expression of genes altered in tau-positive neurons. Significance by mixed-effects linear modeling after FDR correction. Error bars are 95% CI. AD, Alzheimer's disease; Ctl, control; CPM, counts per million; FC, fold change; FDR, false discovery rate; Neg, tau pathology negative; Oligo, oligonucleotide; PART, primary age-related tauopathy; PC, principal component; Pos, tau pathology positive; T−, tau pathology negative; T+, tau pathology positive. Scale bars represent 50 μm. *FDR < 0.05 and **FDR < 0.01.

Author Manuscript Author Manuscript Author Manuscript Author Manuscript

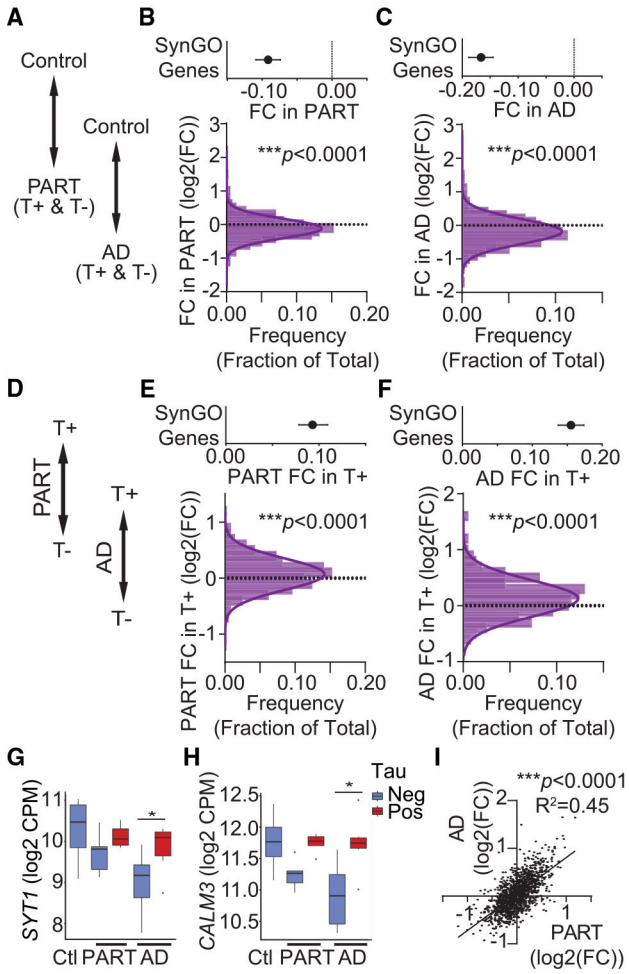

Figure 2. Synaptic gene changes associated with tau pathology in PART and AD

Synaptic genes were identified with SynGO annotation.

(A) Comparison in (B) and (C); control was compared to all neurons in either PART or AD (with and without tau pathology).

(B and C) Decreased synaptic gene expression in PART (B) and AD (C) vs. control shown by fold change of SynGO genes (top) with histogram (below).

(D) Comparison in (E) and (F); tau-positive neurons compared to tau-negative neurons in PART or AD.

(E and F) Increased synaptic gene expression in tau-positive neurons in PART (E) and AD (F) shown by fold change of SynGO genes (top) with histogram (below). (G and H) Representative synaptic and calcium gene changes. Significance by mixed-effects linear model after FDR correction. *FDR < 0.05.

(I) Correlation of fold change in tau-positive neurons in PART and AD (simple linear regression, $p < 0.0001$, $R^2 = 0.45$).

AD, Alzheimer's disease; Ctl, control; CPM, counts per million; FC, fold change; Neg, tau pathology negative; PART, primary age-related tauopathy; Pos, tau pathology positive; T−, tau pathology negative; T+, tau pathology positive. (B, C, E, and F) The curves were generated by Gaussian least squares fit, and the mean is significantly different from 0 by an

extra sum of squares F test; the dotted line is at 0. Error bars are SEM. (G and H) Error bars are 95% confidence interval (CI).

Author Manuscript Author Manuscript Author Manuscript Author Manuscript

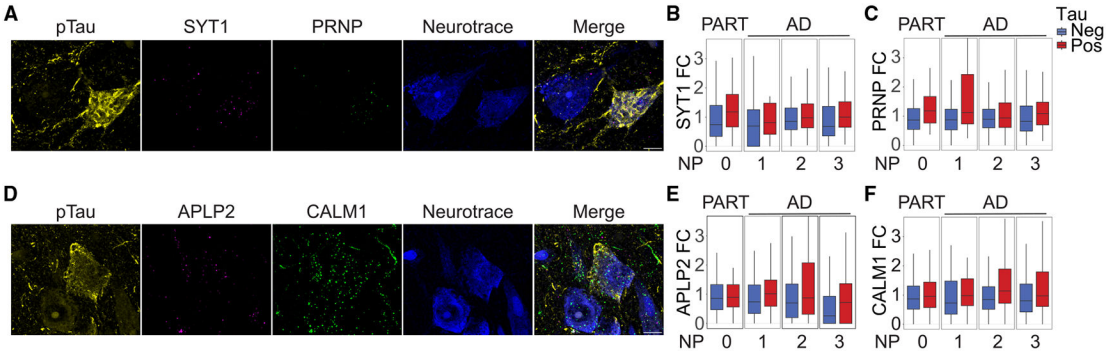

Figure 3. Differential gene expression by tau pathology and neuritic amyloid plaque burden

Gene expression was quantified using hybridization chain reaction (HCR)[35] in cases with varying amyloid plaque burden.

(A and D) Representative HCR images with 2 DEGs measured per section.

(B, C, E, and F) Tau pathology was associated with increased DEG expression (tau effect: B, *SYT1* $p = 0.000131$; C, *PRNP* $p = 1.88–8$; E, *APLP2* $p = 0.000665$; and F, *CALM1* $p = 3.01–5$). Amyloid effect was significant for *APLP2* (E, quadratic amyloid effect: $p = 0.0222$). Amyloid and tau interaction was significant for *PRNP* (C, cubic interaction term: $p = 0.0258$). Statistics by mixed-effects linear model. Neuritic plaque score: 0, none; 1, sparse; 2, moderate; and 3, frequent. Scale bars represent 10 μm.

AD, Alzheimer's disease; FC, fold change compared to tau negative; Neg, tau pathology negative; NP, neuritic plaque score; PART, primary age-related tauopathy; Pos, tau pathology positive. (B–F) Error bars are 95% CI. Points and outliers not shown.

Author Manuscript Author Manuscript Author Manuscript Author Manuscript

Author Manuscript Author Manuscript Author Manuscript Author Manuscript

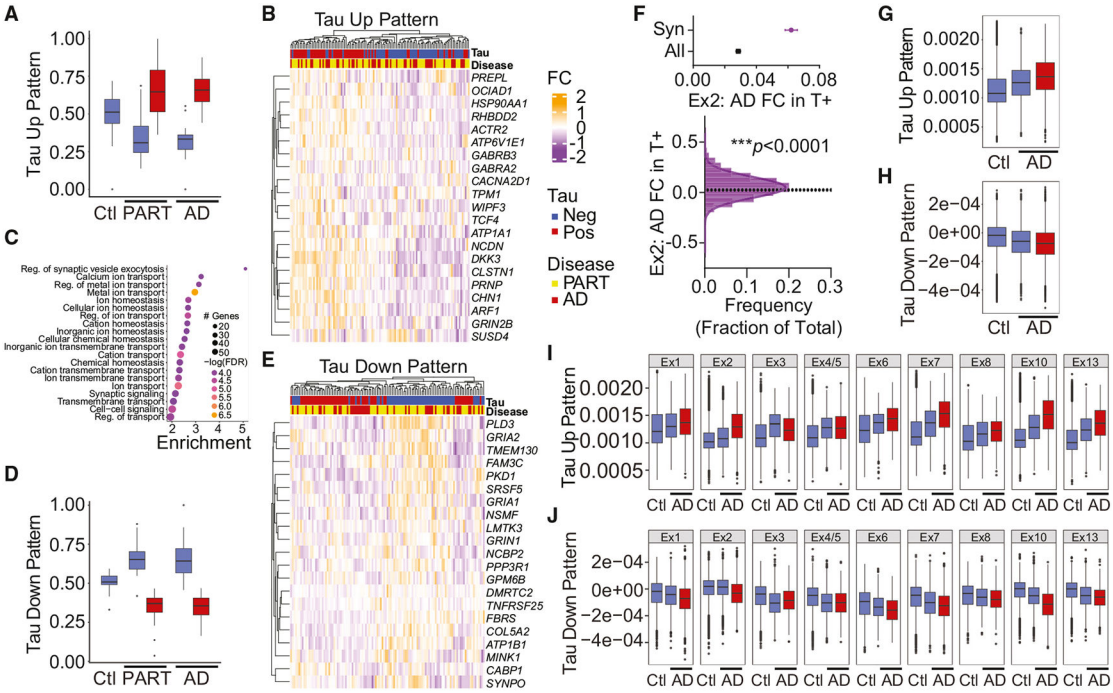

Figure 4. CoGAPS analysis by tau pathology in hippocampal neurons and published cortical neuron dataset

(A and B) Coordinated gene association in pattern set (CoGAPS) score for up-regulated (tau up) pattern by disease group and tau pathology (A) and heatmap of the top 20 genes (B).

(C) Dot plot of biological processes enriched in up-regulated pattern. Dot size reflects number of genes, while color reflects *p* value after FDR correction.

(D and E) CoGAPS score for down-regulated (tau down) pattern by disease group and tau pathology (D) and heatmap of the top 20 genes (E).

(F–J) Data from cortical neurons in AD[20] were analyzed for synaptic gene changes and expression of CoGAPS patterns.

(F) Excitatory neuron group 2 (Ex2: *CUX2-COL5A2*) showing fold change of SynGO genes (top) with histogram (below). The curve was generated by Gaussian least squares fit. Significance is the mean of synaptic genes vs. all genes by an extra sum of squares F test; dotted line is at the mean of all genes.

(G and H) Expression of up-regulated pattern (G) and down-regulated pattern (H) in tau-positive excitatory cortical neurons.

(I and J) Patterns by excitatory neuronal group.

AD, Alzheimer's disease; All, all quantified genes; Ctl, control; FC, log2 fold change; FDR, false discovery rate corrected *p* value; Neg, tau pathology negative; PART, primary age-related tauopathy; Pos, tau pathology positive; Reg., regulation; Syn, synaptic genes; T+, tau positive. (F) Error bars are SEM. (A, D, and G–J) Error bars are 95% CI.

Author Manuscript Author Manuscript Author Manuscript Author Manuscript

KEY RESOURCES TABLE

REAGENT or RESOURCE	SOURCE	IDENTIFIER
Antibodies		
Mouse anti-Phospho-Tau (S202, T205), AT8	ThermoFisher	Cat#MN1020; RRID: AB_223647
Goat anti-mouse IgG1 Alexa 488	ThermoFisher	Cat#A21121; RRID:AB_2535764
Biological samples		
Human hippocampal brain blocks	Johns Hopkins BRC	https://alzresearch.org/resources-for-researchers/
Chemicals, peptides, and recombinant proteins		
eBioscience Antigen Retrieval Solution (10X Tris-EDTA pH 9.0)	ThermoFisher	Cat#00-4956-58
Bio SB ImmunoDNARetriever Solution (20x)	BioSB	Cat#BSB 0021
Proteinase K (20 mg/mL)	ThermoFisher	Cat#AM2546
Proteinase K (20 mg/mL)	New England Biolabs	Cat#P8107S
Heparin	Sigma-Aldrich	Cat#H5515-25KU
Denhardt's Solution	ThermoFisher	Cat#75-001-8
Dextran Sulfate	Sigma-Aldrich	Cat#D6001-10G
Yeast tRNA	Sigma-Aldrich	Cat# R8759-2KU
Custom HCR V3 Probes	Integrated DNA Technologies	Table S8
HCR Amplifier Hairpins: B2-647, B3-546, B4-647, B2-546, B2-488	Molecular Technologies	https://store.molecularinstruments.com/new-bundle/rna-fish
Critical commercial assays		
Alexa Fluor Antibody Labeling Kit	ThermoFisher	Cat # A20185
GeoMx Human Whole Transcriptome Atlas Human RNA for Illumina Systems	NanoString	Cat# GMX-RNA-NGSHuWTA-4
GeoMx Seq Code Pack	NanoString	Cat# GMX-NGS-SEQ-[XX]
GeoMx RNA Slide Prep Kit for FFPE	NanoString	Cat# GMX-PREP-RNAFFPE-12
GeoMx DSP Instrument Buffer Kit	NanoString	Cat#GMX-DSP-BUFF-KIT
Deposited data		
Raw count data and metadata	this study	https://assets.nemoarchive.org/dat-ujtiefy
Cortical AD single cell data	Garcia-Otero et al.[20]	GEO: GSE129308
Software and algorithms		
Fiji/ImageJ	Schindelin et al.[63]	RRID: SCR_002285, https://fiji.sc/
R (version 4.2.2)	R Core Team[64]	RRID: SCR_001905, https://www.r-project.org/
R Studio	Posit Software	https://posit.co/products/open-source/rstudio/
SynGO	SynGO Consortium	RRID: SCR_017330, https://www.syngoportal.org/
ShinyGO (version 0.77)	Ge et al.[65]	RRID: SCR_019213, http://bioinformatics.sdstate.edu/go/
GraphPad Prism	GraphPad Software	RRID: SCR_002798
HCRProbeDesign		https://github.com/gofflab/HCRProbeDesign
Bowtie2	Langmead et al.[66]	https://github.com/BenLangmead/bowtie2
Analysis Code	This study	https://doi.org/10.5281/zenodo.14834548
Other		
NanoString GeoMx Digital Spatial Profiler	NanoString	RRID: SCR_021660

REAGENT or RESOURCE	SOURCE	IDENTIFIER
Illumina NextSeq 2000	Illumina	RRID: SCR_023614
Amaran LED Monolight	BHPhotoVideo	BH#AMAPM022DA10

Author Manuscript
Author Manuscript
Author Manuscript
Author Manuscript